

Three-Dimensional Nanostructures Formed by Single Step, Two-Photon Exposures through Elastomeric Penrose Quasicrystal Phase Masks

Daniel Shir,[†] Hongwei Liao,[†] Seokwoo Jeon,[†] Dong Xiao,[‡] Harley T. Johnson,^{‡,§,¶}
Gregory R. Bogart,[§] Katherine H. A. Bogart,[§] and John A. Rogers^{*,†,‡,¶,||,⊥,§,¶}

Department of Materials Science and Engineering, Department of Mechanical Science and Engineering, Department of Electrical and Computer Engineering, Department of Chemistry, Beckman Institute for Advanced Science and Technology, Materials Research Laboratory, University of Illinois, Urbana–Champaign, Illinois, and Sandia National Laboratories, Albuquerque, New Mexico

Received March 24, 2008; Revised Manuscript Received June 10, 2008

ABSTRACT

We describe the fabrication of unusual classes of three-dimensional (3D) nanostructures using single step, two-photon exposures of photopolymers through elastomeric phase masks with 5-fold, Penrose quasicrystalline layouts. Confocal imaging, computational studies, and 3D reconstructions reveal the essential aspects of the flow of light through these quasicrystal masks. The resulting nanostructures show interesting features, including quasicrystalline layouts in planes parallel to the sample surfaces, with completely aperiodic variations through their depths, consistent with the optics. Spectroscopic measurements of transmission and reflection provide additional insights.

In spite of their many applications, three-dimensional (3D) nanostructures with engineered geometries can be extremely difficult to fabricate. Two optical approaches, one based on coherent interference^{1–4} and the other on two-photon effects,^{5–7} represent the most successful and widely used methods. Interference lithography is attractive because it can form 3D nanostructures over large areas, rapidly. The main disadvantages include the requirement for optical setups that enable independent manipulation of multiple (typically four or more) laser beams, and the ability to produce only a limited range of simple, periodic geometries. Two-photon lithography can fabricate diverse classes of structures, but its standard, serial operation mode requires long fabrication times. In addition, the experimental apparatus is relatively complex, as with interference lithography. A relatively new and simple route to 3D nanofabrication uses single step, two-

photon exposures through phase modulating elements, either in the form of elastomeric masks⁸ or molded relief structures in the photosensitive materials themselves.⁹ In this method, referred to as two-photon proximity field nanopatterning (2ph-PnP), the design of the phase modulating elements can be used to define the geometries of the structures. This 2ph-PnP technique, which represents an improved version of a corresponding one-photon PnP process,^{10,11} provides a valuable complement to other 3D nanofabrication approaches. High speed patterning of 3D structures is possible, with simple setups in which all of the optics can be contained in the phase elements. Although 2ph-PnP does not offer the full flexibility in structure geometry offered by traditional two-photon lithography, it enables a much wider range of possibilities than is practically feasible with interference lithography. Here, we demonstrate 2ph-PnP in an extreme example of this capability, to create a class of quasicrystalline structures that has potential applications in photonics, as an example, where the high rotational symmetry compared to ordinary crystals can provide an increase in photonic bandgaps.¹² In particular, we implement phase elements with Penrose quasicrystal layouts, involving elastomeric masks as well as molded structures of relief. The optics associated with Penrose quasicrystalline masks is not well-understood; it is much more complex than optics associated with masks

* Corresponding author. E-mail: jrogers@uiuc.edu.

[†] Department of Materials Science and Engineering, University of Illinois.

[‡] Department of Mechanical Science and Engineering, University of Illinois.

[§] Sandia National Laboratories.

^{||} Department of Electrical and Computer Engineering, University of Illinois.

[⊥] Department of Chemistry, University of Illinois.

[¶] Beckman Institute for Advanced Science and Technology, University of Illinois.

[⊥] Materials Research Laboratory, University of Illinois.

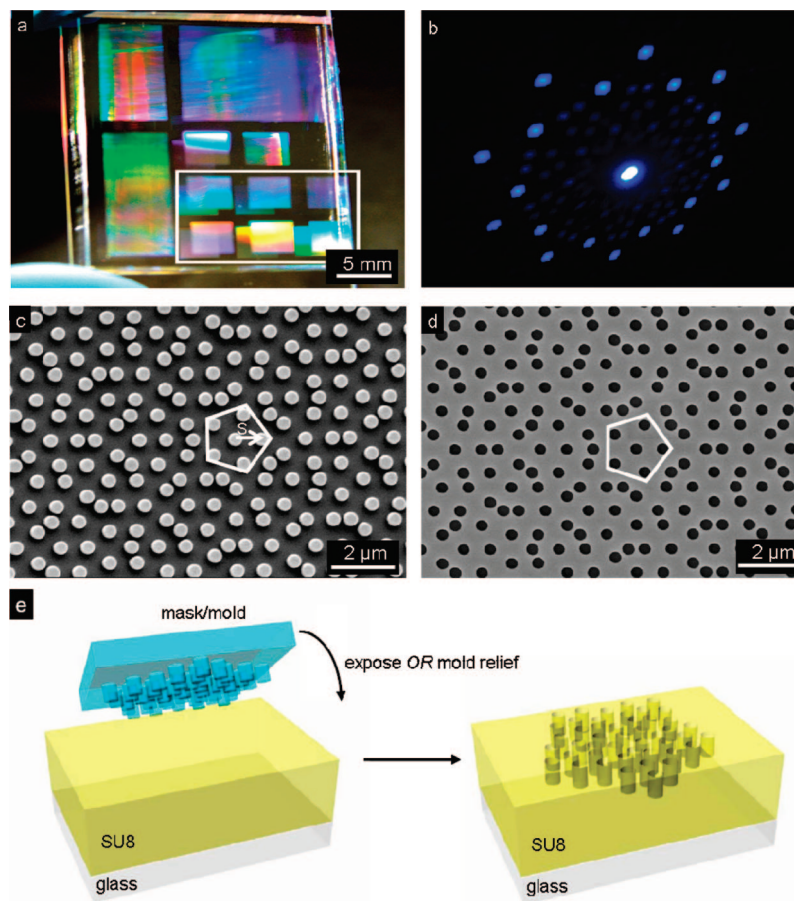


Figure 1. Optical and scanning electron microscope (SEM) images and schematic illustrations of aspects associated with two-photon proximity field nanopatterning (PnP) using quasicrystalline phase masks. (a) Optical image of a PDMS phase mask. The white rectangle highlights the regions that contain posts in two-dimensional, Penrose quasicrystalline geometries. (b) Far-field diffraction pattern associated with passage of 355 nm laser light through a region of this mask that represents Penrose tiling with characteristic distance of 800 nm, post diameters of 200 nm and heights of 400 nm. (c,d) High resolution SEM images of a representative region of a phase mask and layer of photopolymer embossed with this mask, respectively. (e,f) Schematic illustrations of the use of the mask for a standard PnP process and for embossing a layer of photopolymer in a maskless implementation of PnP, respectively.

characterized by a well-defined unit cell. The 3D nanostructures that can be formed with such Penrose masks have similarly complex and unusual layouts, in our case consisting of continuous stacks of 5-fold symmetric quasicrystalline layouts in planes parallel to the surface of the mask, together with a complete lack of identifiable symmetry in planes perpendicular to the mask surface. Such unique types of nanostructures would be impossible to form with any other technique, except certain classes of slow, direct-write methods.⁵ We begin with an overview of the Penrose phase designs and their use in the patterning process. Experimental measurements and theoretical modeling reveal the key aspects of the optics of these unusual elements. Several representative 3D structures that result from their implementation in the 2ph-PnP patterning process are presented. Wavelength-dependent transmission and reflection measurements, together with approximate modeling of the responses, reveal some of their optical properties.

Figure 1a shows an image of a typical elastomeric phase mask used in this work. The fabrication of these phase elements involves casting and curing prepolymers of two types of materials based on poly(dimethylsiloxane) (PDMS)

against substrates with structures of relief in the geometry of Penrose quasicrystals.^{13–16} The process began with casting a relatively high modulus (~ 10 MPa) type of PDMS (Gelest, Morrisville, PA) followed by a low modulus (~ 2 MPa) variant (Sylgard 184, Dow-Corning) against patterns of cylindrical holes in photoresist, defined on a silicon wafer by deep ultraviolet (UV; 248 nm) projection mode photolithography in procedures similar to those described previously.¹¹ The high modulus PDMS yields high quality relief structures, without the mechanical collapse and other failure modes that often occur in narrow and tall features on low modulus masks. The backing layer of low modulus PDMS provides a mechanically tough “handle” that avoids the need to handle directly the relatively brittle high modulus material.^{11,16} Each mask supports several different regions that correspond to various two-dimensional (2D) Penrose quasicrystal lattices of cylindrical posts, with radii (r) of 200 nm, heights (h) of 400 nm, and different characteristic separations ranging from 600 to 1500 nm, as highlighted by the rectangle in Figure 1a. The characteristic separation (S) represents the distance from the center of a local 5-fold symmetric structure to the nearest neighbor symmetry point,

as indicated by the white arrow in Figure 1c. This distance is proportional to a fundamental length scale, the golden ratio $\pi = (\sqrt{5} + 1)/2$. The work described here uses $S = \pi/2 \mu\text{m} = 810 \text{ nm}$, although the masks support patterns with S between 0.6 and 1.5 μm . The lattices represent quasicrystals constructed from two Penrose rhombi assembled according to certain matching rules.¹⁷ The tiling incorporates structures (i.e., pentagons formed by combination of 5 Penrose rhombi) with 5-fold symmetry in layouts that correspond to quasi-periodic patterns with global 10-fold rotational symmetry. These quasicrystalline phase masks generate far field diffraction patterns that include hundreds of beams, with 10-fold symmetry (Figure 1b; 355 nm light projected onto a white card to produce blue fluorescent spots). Although the designs are different, these qualitative features are similar to other classes of quasicrystal phase masks that were recently implemented in a one photon PnP process, in independent work.¹⁸

The overlap of these beams near the surface of the mask results in a complex pattern of intensity that can be exploited for patterning in the 2Ph-PnP process. Two procedures were used. The first involved establishing conformal contact of the PDMS mask with the flat surface of a solid layer of a transparent, photosensitive polymer, exposing the polymer by passing UV light through the mask, removing the mask and, finally, developing away the unexposed regions.¹¹ The second procedure used the mask as a mold to emboss patterns of relief into the photopolymer.⁹ Similar exposure and development procedures carried out with the embossed photopolymer (i.e., without the PDMS mask) completed the fabrication, in a process referred to as maskless 2ph-PnP. Figure 1e,f provides schematic illustrations of these two patterning strategies. This procedure has advantages in that (i) high index photopolymers can provide enhanced phase modulation compared with that of PDMS masks, for the same relief depth, which is important for demanding feature sizes such as those reported here, and (ii) high order diffracted beams can couple efficiently into the bulk of the photopolymer, because of the absence of Fresnel reflections that can occur with the use of a mask, which is important for achieving high contrast ratio exposures. Figure 1c,d shows high resolution scanning electron microscope (SEM) images of a representative region of a mask and embossed surface of a layer of photopolymer, respectively. A pentagon drawn in each frame highlights the basic 5-fold symmetry. The processing steps for both cases are similar to those described previously for nonquasicrystalline masks.^{9–11} Briefly, a layer ($\sim 10 \mu\text{m}$) of negative tone epoxy photoresist (SU-8, Microchem Corp.) spin-cast (2500 rpm, 30 s) onto a glass slide and baked (65 °C for 5 min and 95 °C for 10 min) to remove the solvent served as the photopolymer. The molding process consisted of softening this layer with a small amount of ethanol and then embossing it with a PDMS phase mask.⁹

The exposures exploited two-photon effects generated using the high peak power, collimated output of an amplified Ti:sapphire laser (Spectra-Physics, Spitfire Pro), with wavelength of 800 nm, average power of $\sim 2 \text{ W}$, repetition rate of 1 kHz, and pulse width of $\sim 140 \text{ fs}$. The coherence length

of these laser pulses is $\sim 30 \mu\text{m}$ in the SU8, which is substantially larger than the sample thickness. This limited coherence length can be important in attempts to pattern thicker structures. A lens with a focal length of 400 mm provided a beam with a small convergence angle ($< 10 \text{ mrad}$), and an exposure region with a spot size of 3–4 mm, from an output beam with diameter $\sim 1 \text{ cm}$. The use of circularly polarized light avoided polarization induced directional anisotropies in the intensity patterns that can appear due to polarization dependent diffraction from subwavelength masks.^{8,9} After exposure, the SU-8 film was baked (75 °C for 6 min), developed (2 h in SU-8 developer), and supercritically dried to complete the fabrication. The quadratic relationship between intensity and dose associated with the two-photon process yields high contrast exposures and robust, 3D nanostructures with levels of open porosity and classes of geometries that are impossible to achieve with single photon effects.^{8,9} This exposure condition, then, represents a critically important aspect of the results presented here, and enables structures with features (e.g., open porosity) and geometries that cannot be achieved in the corresponding one photon process.^{8,9}

Before examining the nanostructures that result from this process, it is useful to consider aspects of the unusual optics associated with transmission through the Penrose masks. For this purpose, we exposed SU8 doped with a fluorophore (Coumarin 6 (C6)) that has pH sensitive emission characteristics.¹⁹ In the unexposed and exposed regions, the C6 fluoresces at $\sim 490 \text{ nm}$ and $\sim 550 \text{ nm}$, respectively. Confocal imaging (TCS SP2, Leica Microsystems) of emission at 550 nm, stimulated by 514.5 nm light from an Ar ion laser, from a sample of exposed (but not developed) SU8/C6, yielded three-dimensional reconstructions of the distributions of intensity associated with the PnP process. We used the microscope in an oil immersion mode, with a 63 \times objective lens capable of providing resolution of $\sim 170 \text{ nm}$ and $\sim 320 \text{ nm}$ in plane of the surface of the sample (x,y plane, Figure 2a) and along the direction perpendicular to this plane (z , Figure 2a), respectively. Figure 2 shows results, in the form of images in the x,y plane of a sample created using the maskless PnP process, evaluated at different z distances. A pentagon in each frame highlights the local 5-fold symmetry. The intensity distributions maintained this symmetry throughout this range of z depths; the z dependence is, however, complex and not simply periodic.

The full 3D optics of this system are challenging to model directly, because of the quasicrystalline geometry. An accurate picture requires, in particular, direct modeling of an entire mask (or large region of a mask), due to the absence of a unit cell that could otherwise enable periodic boundary conditions. As a simple approximation that can be accomplished relatively easily, we simulated a finite size system with in-plane geometry consistent with the Penrose tiling, for the case of steady state light propagation through an embossed layer of SU8. The relief had the ideal 5-fold Penrose symmetry (Figure 3a, right frame) of the experimental system described previously. The cylindrical wells (filled with air) of the embossed structure had diameters of

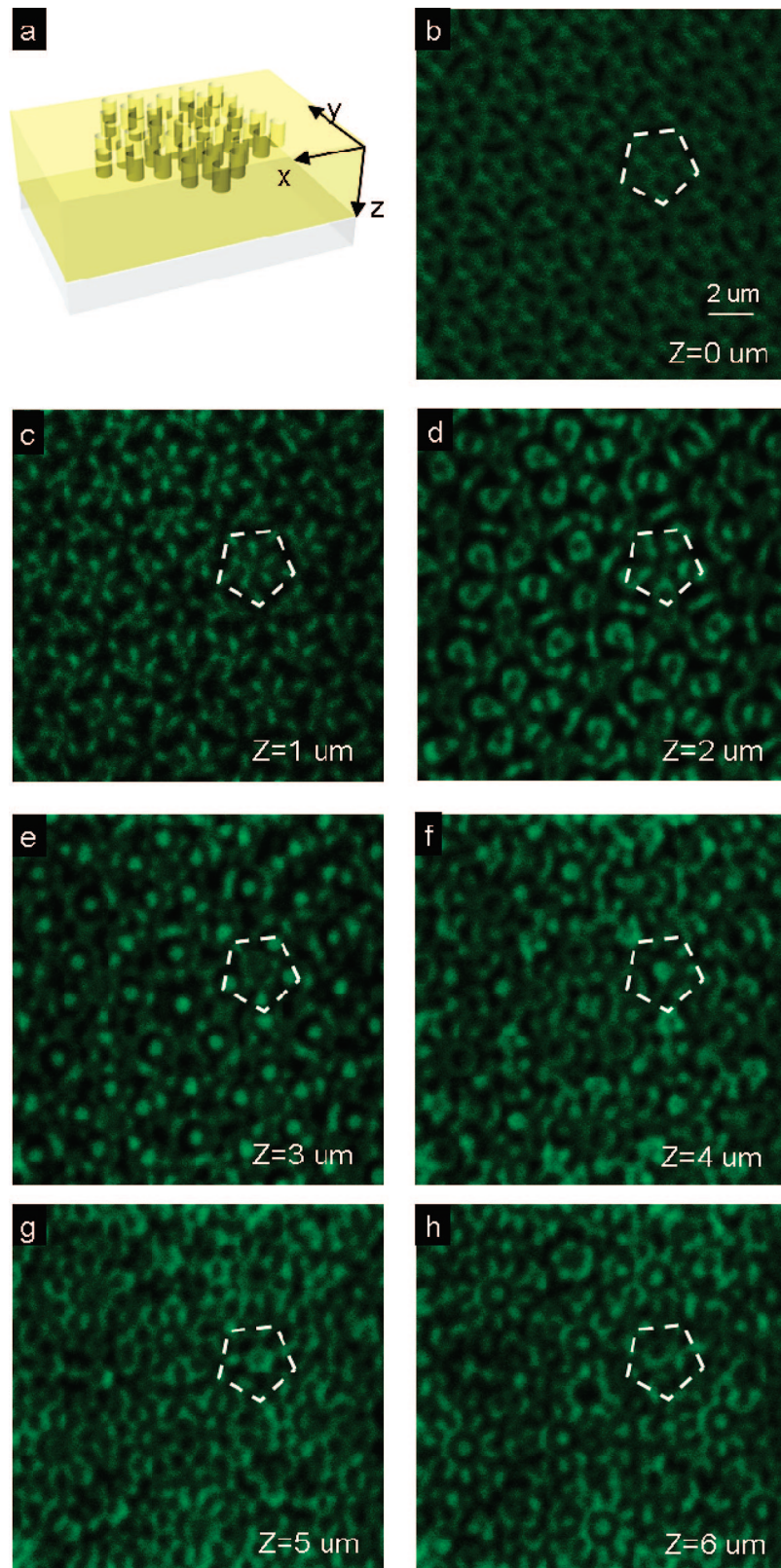


Figure 2. Confocal images that reveal the three-dimensional distributions of intensity that form upon passage of light through a molded photopolymer layer similar to that shown in Figure 1d. (a) Schematic illustration of this photopolymer layer. (b–h) Confocal images in the x – y plane at increasing z distances from the top surface of the sample. The step size is $1 \mu\text{m}$.

200 nm and depths of 400 nm, consistent with the experiment. The total thickness of the SU8 was $3 \mu\text{m}$; the index of refraction was 1.59 (at 800 nm), without any scattering or absorption losses. Second order absorbing boundary

conditions were used at the top surface (where light was incident) and at the bottom surface. The tangential electric field was set to zero at all 10 sidewalls of the simulated system. This symmetry boundary condition approximates a

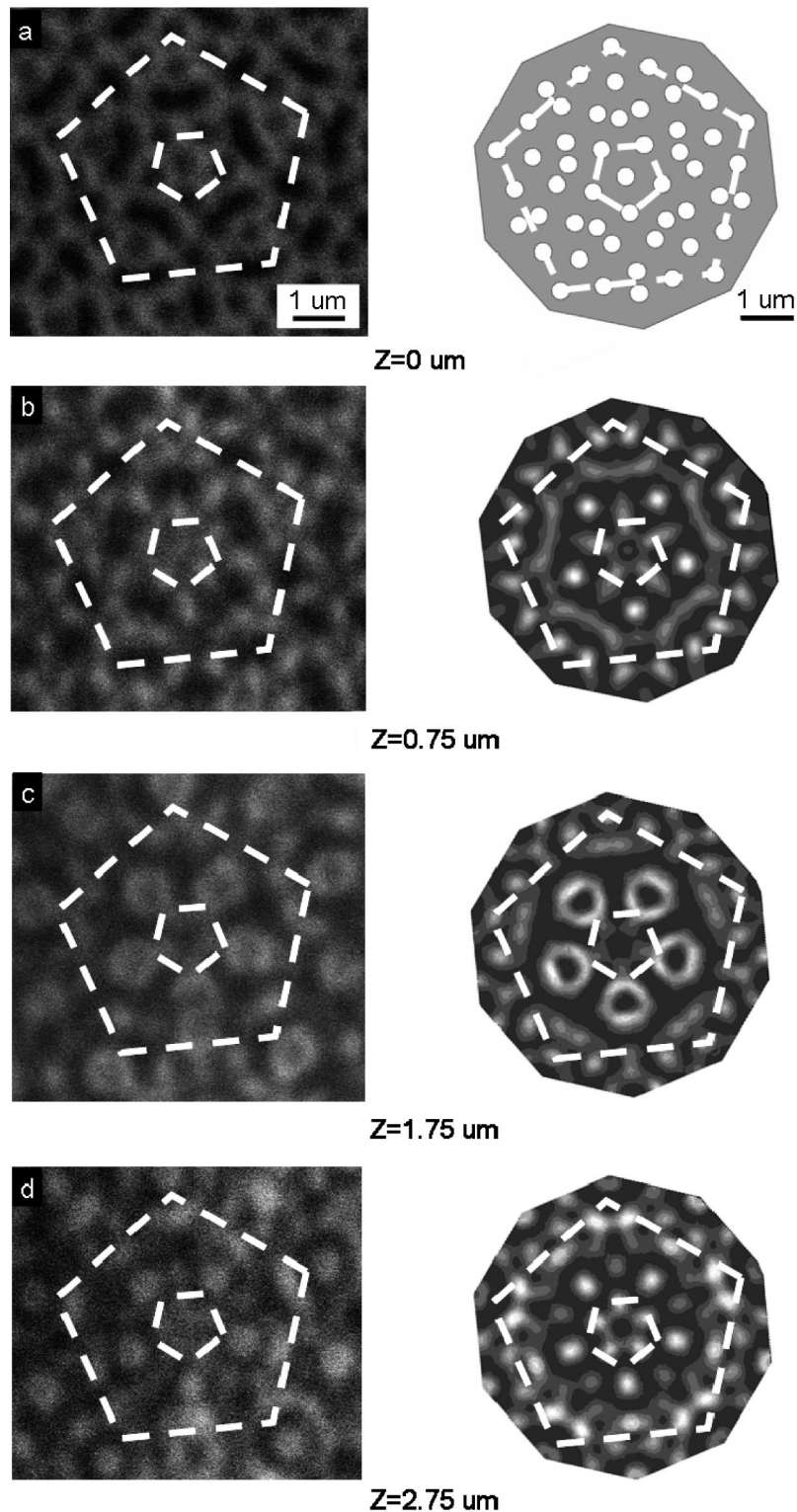


Figure 3. Comparison of confocal images (left) and computer simulations (right) at different distances (z) from the surface of the sample. (a) Confocal images of the molded surface (left) and the geometry of the periodic structure used in the finite element modeling (right). (b–d) Confocal images (left) and simulation results (right) at $z = 0.75, 1.75,$ and $2.75 \mu\text{m}$, respectively.

reasonable lateral area (given limited computational resources) of the experimental system, for which it is not possible to construct a true periodic unit cell. The electric field polarization is set to be circularly polarized, matching the experimental condition. The right-hand frames of Figure 3b–d show calculations of the square of the time averaged

total energy density in the x,y plane at various z positions corresponding to the confocal images (Figure 3, left-hand frames). As an aid to the eye, two pentagons of different sizes highlight the symmetries. We observe reasonable agreement between theory and experiment, particularly in the central regions of the simulations and for depths $< \sim 2$

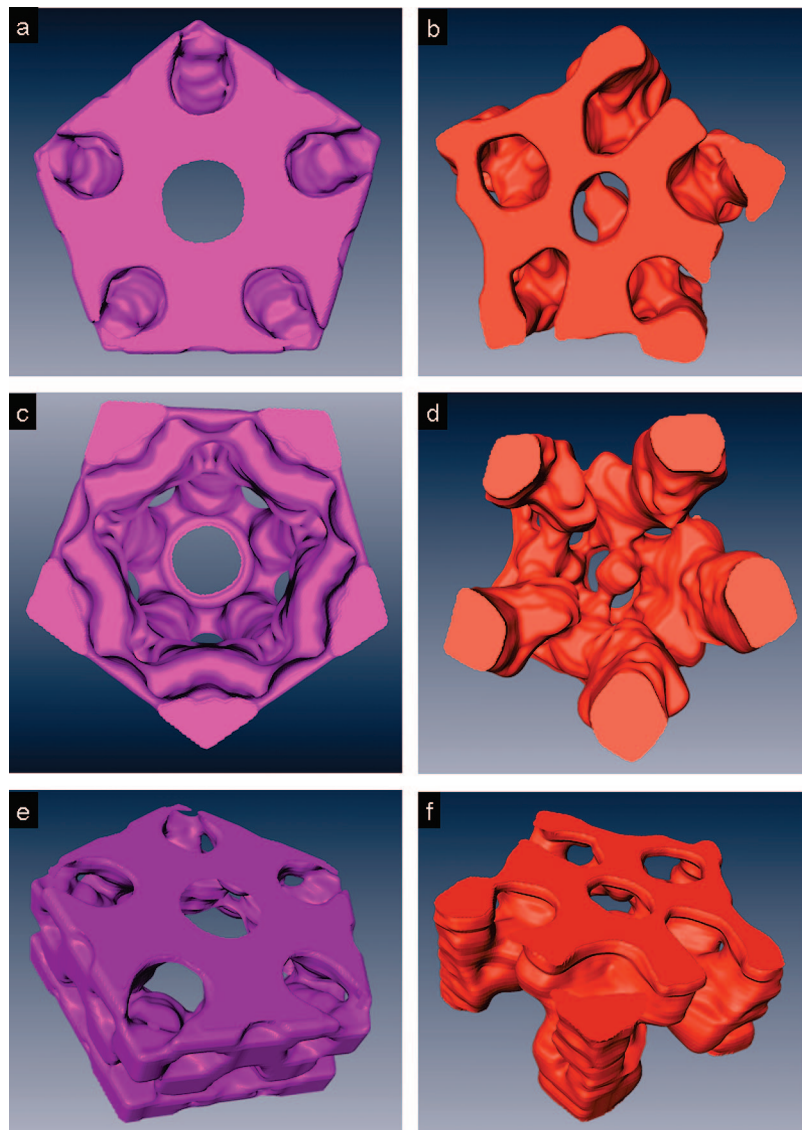


Figure 4. Three dimensional reconstructions created from confocal images (right) and simulation results (left). (a,b) Top views, (c,d) back views, and (e,f) angled views of the 3D reconstructions. Intensity thresholding yields solid structures that approximate resist structures that form in the PnP process.

μm , thereby validating the approximations associated with the modeling. The Talbot distances for grating periodicities of 600 and 1500 nm are respectively ~ 1100 nm and ~ 8700 nm, for an incident wavelength of 800 nm and refractive index of 1.59. The characteristic separation associated with the simulated system is ~ 800 nm corresponding to a Talbot distance of ~ 2300 nm. Because the mask lacks any long-range periodicity, however, there is a complete absence of Talbot planes in the actual sample.

The measured and simulated results allow reconstruction of the full 3D intensity distributions using appropriate software tools (Amira, Visage Imaging, Inc.). Median and smooth filtering, combined with intensity thresholds, can simulate, approximately, the development process to yield predictions for the 3D structure geometries. The intensity threshold provides a simple way to connect intensity distributions to solid forms, with good agreement in PnP experiments that use periodic masks.⁸⁻¹¹ The median filter averages over 5 pixels, or approximately 50 nm in the image,

while the smooth filter produces clean boundaries between polymer and air by smoothing the rough boundaries in 3D reconstruction from layers of 2D slices. These two procedures eliminate spatial frequencies in the solid structures that exceed those observed experimentally with SU8. This process was performed on measured and simulated results consisting of 27 data images with step sizes along z of $0.125 \mu\text{m}$. Figure 4 presents results of top, bottom, and angled views that highlight the good, semiquantitative agreement between theory (left) and experiment (right) and the complex nanostructures that are expected to result from the quasicrystal PnP process.

The actual 3D structures have features consistent with the optics. Figure 5 presents the results of PnP using the mask based process. Figure 5a,c shows magnified and large area views, respectively, of the top surface region of a typical sample. The pentagon highlights the local 5-fold symmetry of the mask and the optics. The white arrows indicate a few of the relatively small number of defects visible in the

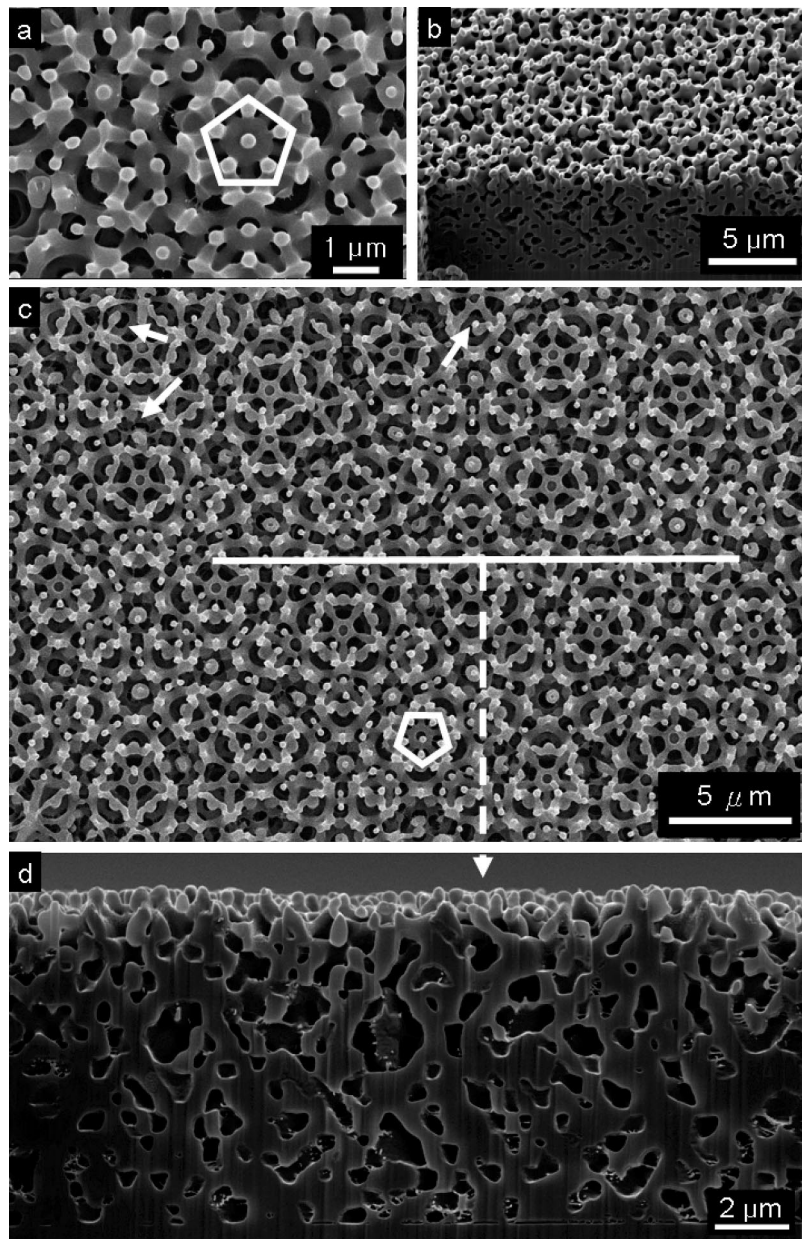


Figure 5. SEM images of 3D nanostructures formed by two-photon PnP using a PDMS Penrose quasicrystalline phase mask. (a,b) High resolution top and angled views of the top surfaces of the structures, respectively. (c) Large area top view, with arrows that point to some structural defects. (d) FIB-cut cross-sectional view.

structure. The overall lateral dimensions of the samples were 3 mm by 3 mm, limited only by the size of the mask and the exposure beam. The structure in the top layer, as revealed in Figure 5a,c is dominated by an effective type of sub-wavelength focusing, similar to that observed in periodic masks,¹³ in which bright and dark areas appear next to the raised and recessed regions of the mask, respectively. The structure, then, in this part of the sample matches the geometry of the mask. Figure 5b,d shows angled and cross-sectional views, respectively. A horizontal line in Figure 5c identifies the approximate positions of the cross-sectional cut. Focused ion beam (FIB) sectioning produced clean cuts through the sample for these images. (Atomic layer deposition of ~ 2 nm Al_2O_3 onto the 3D structure minimized damage during high energy ion beam bombardment.) These cross-sectional views indicate a lack of periodicity along the

depth direction, consistent with the optics. Figure 6 presents images similar to those in Figure 5, but for the case of a structure formed with the maskless PnP process. Here, the structure of the top surface is determined not only by the optics but also by the material structures and differential development conditions associated with the embossed relief. We observed no defects in this surface region. As with the structure of Figure 5, the cross-sectional views reveal a lack of any simple periodic variation in the structure geometry with depth. A horizontal line in Figure 6c provides the location of the FIB cut.

Because of the interest in the optical properties of 3D quasicrystals and to gain further insights into the geometries of our structures, we performed normal incidence transmission (T) and reflection (R) measurements with a Fourier transform infrared (FTIR) spectrometer (Bruker Optics Inc., model

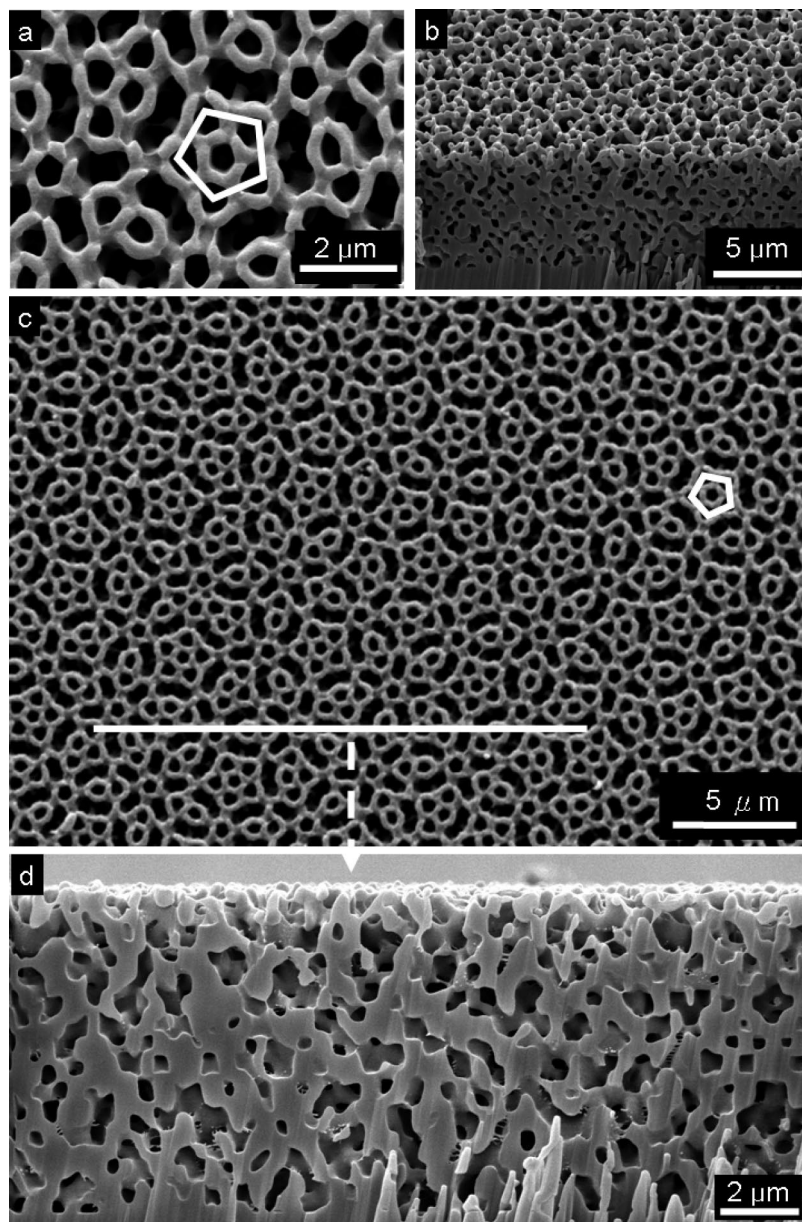


Figure 6. SEM images of 3D nanostructures formed by two-photon PnP using the maskless process. (a,b) High resolution top and angled views of the top surfaces of the structures, respectively. (c) Large area top view. (d) FIB-cut cross-sectional view.

Hyperion 1000). The samples consisted of structures on glass coverslips. The spectrometer was calibrated in transmission and reflection measurements using a bare glass coverslip (substrate) and a silver mirror (reflection $>96\%$ from 0.5 to 4 μm), respectively. The measurement spot size was 75 μm with a $4\times$ objective lens and a 0.45 mm diameter aperture. T/R spectra are shown in Figure 7. Samples exhibit a gradual reduction in transmission at shorter wavelengths, but without any other distinct features. Visual inspection of transmission of visible laser light through the sample indicated diffuse scattering, without any significant coherent diffraction. Although the transmission spectra show some structure, the overall trends follow expected behavior due to random scattering (i.e., inversely proportional to the fourth power of the wavelength, as shown by the curve “T-scattering” in Figure 7). Reflection measurements throughout the 3D structures show no consistent, distinct peaks, indicating the

lack of periodicity in the vertical direction. This observation is consistent with the optics of the fabrication process and from the SEM images.

In summary, this paper demonstrates how two-photon exposure techniques can be implemented with quasicrystalline masks to yield 3D nanostructures with highly unusual geometries. The optics of the masks and the transmission properties of the structures are both shown to be consistent with approximate models. The use of such models was found to be helpful for process evaluation, despite their inherent inability to describe completely the optical properties of the quasi-crystal. The high speed, large area capabilities of the fabrication methods could facilitate use of these unusual structures in practical applications not only in photonics but also in areas of catalysis, microfluidics, drug release, and others that can benefit from well-controlled nanoporous materials. Interest in the photonic properties of these unique

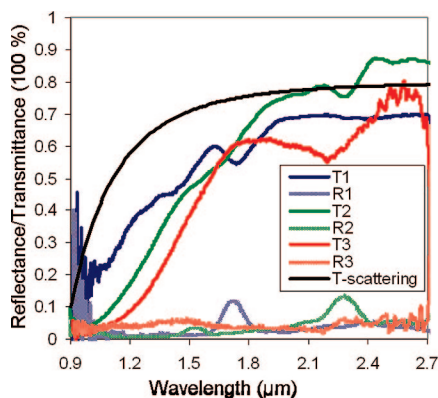


Figure 7. Reflection/transmission spectra collected from a 3D nanostructure formed using the maskless PnP process with a quasicrystalline Penrose mold. Curves (T1, T2, T3, and R1, R2, R3) correspond to measurements of different locations of a representative structure. The black curve labeled T-scattering corresponds to a simple calculation of wavelength dependent scattering in a random media.

structures might be strongest for propagation in the quasicrystalline planes (i.e. x , y planes). In addition, the extreme tortuosity and large surface areas associated with the interconnected pore structures in the out of plane direction may also make them useful for applications in fluidics, chromatographic separations, and controlled release. Exploring these and other possibilities represents the focus of current work.

Acknowledgment. We thank T. Banks and K. Colravy for help with processing using facilities at the Materials Research Laboratory. This work is supported by the DOE through Grant DE-FG02-07ER46471 and Sandia National Laboratories, a multiprogram laboratory operated by Sandia Corporation, a Lockheed Martin Company, for the U.S. Department of Energy's National Nuclear Security Administration under Contract No. DE-AC04-94AL85000. The facilities included the Materials Research Laboratory, Uni-

versity of Illinois, which is partially supported by the U.S. Department of Energy under Grants DE-FG02-07ER46453 and DE-FG02-07ER46471.

Supporting Information Available: Additional experimental and theoretical details. This material is available free of charge via the Internet at <http://pubs.acs.org>.

References

- (1) Campbell, M.; Sharp, D. N.; Harrison, M. T.; Denning, R. G.; Turberfield, A. J. *Nature* **2000**, *404*, 53–56.
- (2) Yang, S.; Megens, M.; Aizenberg, J.; Wiltzius, P.; Chaikin, P. M.; Russel, W. B. *Chem. Mater.* **2002**, *14*, 2831–2833.
- (3) Divliansky, I.; Mayer, T. S.; Holliday, K. S.; Crespi, V. H. *Appl. Phys. Lett.* **2003**, *82*, 1667–1669.
- (4) Ullal, C. K.; Maldovan, M.; Thomas, E. L.; Chen, G.; Han, Y.-J.; Yang, S. *Appl. Phys. Lett.* **2004**, *84*, 5434–5436.
- (5) Sun, H.-B.; Kawata, S. *Adv. Polym. Sci.* **2004**, *170*, 169–273.
- (6) Kondo, T.; Matsuo, S.; Juodkazis, S.; Misawa, H. *Appl. Phys. Lett.* **2001**, *79*, 725–727.
- (7) Grier, D. G. *Nature* **2003**, *424*, 810–816.
- (8) Jeon, S.; Malyarchuk, V.; Rogers, J. A.; Wiederrecht, G. P. *Opt. Exp.* **2006**, *14* (6), 2300–2308.
- (9) Jeon, S.; Shir, D. J.; Nam, Y. S.; Nidetz, R.; Highland, M.; Cahill, D. G.; Rogers, J. A.; Su, M. F.; El-Kady, I. F.; Christodoulou, C. G.; Bogart, G. R. *Opt. Exp.* **2007**, *15* (10), 6358–6366.
- (10) Shir, D. J.; Jeon, S.; Liao, H.; Highland, M.; Cahill, D. G.; Su, M. F.; El-Kady, I. F.; Christodoulou, C. G.; Bogart, G. R.; Hamza, A. V.; Rogers, J. A. *J. Phys. Chem. B* **2007**, *111*, 12945–12958.
- (11) Jeon, S.; Park, J.-U.; Cirelli, R.; Yang, S.; Heitzman, C. E.; Braun, P. V.; Kenis, P. J. A.; Rogers, J. A. *Proc. Natl. Acad. Sci. U.S.A.* **2004**, *101*, 12428–12433.
- (12) Zoorob, M. E.; Charlton, M. D. B.; Parker, G. J.; Baumberg, J. J.; Netti, M. C. *Nature* **2000**, *404*, 740–743.
- (13) Xia, Y.; Whitesides, G. M. *Angew. Chem., Int. Ed. Engl.* **1998**, *37*, 550–575.
- (14) Xia, Y.; Rogers, J. A.; Paul, K. E.; Whitesides, G. M. *Chem. Rev.* **1999**, *99*, 1823–1348.
- (15) Schmid, H.; Michel, B. *Macromolecules* **2000**, *33*, 3042–3049.
- (16) Odom, T. W.; Love, J. C.; Wolfe, D. B.; Paul, K. E.; Whitesides, G. M. *Langmuir* **2002**, *18*, 5314–5320.
- (17) Radin, C. *J. Stat. Phys.* **1999**, *95*, 827–833.
- (18) Bitá, I.; Choi, T.; Walsh, M. E.; Smith, H. I.; Thomas, E. L. *Adv. Mater.* **2007**, *19*, 1403–1407.
- (19) Ray, K.; Mason, M. D.; Grober, R. D.; Pohlert, G.; Staford, C.; Cameron, J. F. *Chem. Mater.* **2004**, *16*, 5726–5730.

NL080841K